Published in final edited form as:
Bioconjug Chem. 2011 August 17; 22(8): 1650–1662. doi:10.1021/bc200227d.

Multivalent Bifunctional Chelator Scaffolds for Gallium-68 Based Positron Emission Tomography Imaging Probe Design: Signal Amplification *via* Multivalency

Ajay N. Singh[1,†], **Wei Liu**[1,2,†], **Guiyang Hao**[1], **Amit Kumar**[1], **Anjali Gupta**[1], **Orhan K. Öz**[1], **Jer-Tsong Hsieh**[3], and **Xiankai Sun**[1,4,*]

[1]Department of Radiology, University of Texas Southwestern Medical Center, Dallas, Texas, USA

[2]State Key Lab of Crystal Materials, Shandong University, Jinan, Shandong, P. R. China

[3]Department of Urology, University of Texas Southwestern Medical Center, Dallas, Texas, USA

[4]Advanced Imaging Research Center, University of Texas Southwestern Medical Center, Dallas, Texas, USA

Abstract

The role of the multivalent effect has been well recognized in the design of molecular imaging probes towards the desired imaging signal amplification. Recently we reported a bifunctional chelator (BFC) scaffold design, which provides a simple and versatile approach to impart multivalency to radiometal based nuclear imaging probes. In this work, we report a series of BFC scaffolds ($^{t}Bu_3$-**1**-COOH, $^{t}Bu_3$-**2**-$(COOH)_2$ and $^{t}Bu_3$-**3**-$(COOH)_3$) constructed on the framework of 1,4,7-triazacyclononane-1,4,7-triacetic acid (NOTA) for ^{68}Ga-based PET probe design and signal amplification *via* multivalent effect. For proof of principle, a known integrin $\alpha_v\beta_3$ specific ligand (c(RGDyK)) was used to build the corresponding NOTA conjugates (H_3**1**, H_3**2**, and H_3**3**), which present 1 – 3 copies of c(RGDyK) peptide, respectively, in a systematic manner. Using the integrin $\alpha_v\beta_3$ binding affinities (IC_{50} values), the enhanced specific binding was observed for multivalent conjugates (H_3**2:** 43.9 ± 16.1 nM; H_3**3**: 14.7 ± 5.0 nM) as compared to their monovalent counterpart (H_3**1:** 171 ± 60 nM) and the intact c(RGDyK) peptide (204 ± 76 nM). The obtained conjugates were efficiently labeled with $^{68}Ga^{3+}$ within 30 min at room temperature in high radiochemical yields (> 95%). The *in vivo* evaluation of the labeled conjugates, ^{68}Ga-**1**, ^{68}Ga-**2** and ^{68}Ga-**3**, was performed using male severe combined immunodeficiency (SCID) mice bearing integrin $\alpha_v\beta_3$ positive PC-3 tumor xenografts (n = 3). All ^{68}Ga -labeled conjugates showed high *in vivo* stability with no detectable metabolites found by radio-HPLC within 2 h post-injection (p.i.). The PET signal amplification in PC-3 tumor by multivalent effect was clearly displayed by the tumor uptake of the ^{68}Ga-labeled conjugates (^{68}Ga-**3:** 2.55 ± 0.50%ID/g; ^{68}Ga-**2**: 1.90 ± 0.10 %ID/g; ^{68}Ga-**1**: 1.66 ± 0.15 %ID/g) at 2 h p.i. In summary, we have designed and synthesized a series of NOTA-based BFC scaffolds with signal amplification properties, which may find potential applications in diagnostic gallium radiopharmaceuticals.

[*]Correspondence to Xiankai Sun, Ph.D., Department of Radiology and Advanced Imaging, Research Center, University of Texas Southwestern Medical Center at Dallas, 2201 Inwood Road, Texas 75390-8542, USA; Xiankai.Sun@UTSouthwestern.edu.
[†]A. Singh and W. Liu contributed equally to this work.

Supporting Information Available: [Figure S1–2 and Table S1–3] This material is available free of charge via the Internet at http://pubs.acs.org.

Introduction

Positron emission tomography (PET), a nuclear imaging technique, has become a standard-of-care tool for diagnosis, staging treatment planning, and therapeutic efficacy monitoring of patients with cancer or other diseases.[1–5] In addition to clinical applications, PET is also widely used in laboratory research to study the underlying mechanisms of diseases and to facilitate the discovery of new treatments.[6] Development and application of PET imaging probes from the standard PET radionuclides (^{15}O: $t_{1/2}$ = 2.04 min; ^{13}N: $t_{1/2}$ = 9.96 min; ^{11}C: $t_{1/2}$ = 20.4 min; and ^{18}F: $t_{1/2}$ = 110 min) suffer from the short half-lives of the radionuclides, which mandates the presence of a radiochemistry laboratory in the close proximity of a cyclotron facility.[7] To date, PET probe development using non-standard PET radionuclides (e.g. ^{64}Cu, ^{68}Ga, ^{89}Zr, ^{124}I) has drawn considerable interest given its independence to a cyclotron facility.[8, 9] Among the non-standard PET radionuclides, ^{68}Ga ($t_{1/2}$ = 68 min, 89% β^+, $E_{\beta+\ max}$ =1.92 MeV, 11% EC) has the most clinical significance as it can be obtained on as needed basis from a bench-top ^{68} Ge/^{68}Ga generator system thereby negating the onsite cyclotron requirement.[10–14] Compared to ^{18}F, the shorter half-life of ^{68}Ga is not necessarily a hindrance in preclinical or clinical applications because its well-established coordination chemistry enables a rapid radiolabeling with high radiochemical yields,[15, 16] which provides an opportunity to develop commercial kits to prepare PET probes onsite for diagnostic and prognostic imaging of diseases.

A macrocyclic chelator, 1,4,7-triazacyclononane-1,4,7-triacetic acid (NOTA), and its derivatives are particularly suitable for ^{68}Ga incorporation due to their fast and efficient radiolabeling and *in vivo* stability (Figure 1).[10, 11, 16] The stability of Ga(III)-NOTA complex results from the perfect hole-size match between the NOTA cavity and Ga^{3+} metal ion, which is accentuated by the tight embrace of the three coordinating carboxylate groups (Figure 1).[17–23] However, application of NOTA for a targeted PET probe design is restricted because of its limited bifunctionality. Once the pendent carboxylic acid of the NOTA is conjugated with a targeting vector, the coordinating ability of the NOTA with ^{68}Ga is compromised due to the loss of a coordinating pendent carboxylate group. Several NOTA derivatives such as S-2-(4-Isothiocyanatobenzyl)-1,4,7-triazacyclononane-1,4,7-triaceticacid (NOTA-Bn-SCN), 1,4,7-triazacyclononane-1-succinic acid-4,7-diacetic acid (NODASA) and 1-(1-Carboxy-3-carbo-*tert*-butoxypropyl)-4,7-(carbo*tert*-butoxymethyl)-1,4,7-triazacyclononane (NODAGA) have been designed to circumvent this problem.[15, 18, 19, 23, 24] The general concept of these modifications is the presence of an additional functionality on the macrocylic core for vector conjugation, while preserving NOTA's capability of stable Ga^{3+} chelation (Figure 1).

A PET probe design is aimed to facilitate the accurate detection and quantitative analysis of a disease state, which requires high imaging sensitivity and specificity of the designed probe towards the target. To date, the multivalent effect has become a well-accepted concept in the design of molecular imaging probes for specific signal amplification by enhancing the binding affinity of a probe to the specific cell surface receptor.[25] The most common way to incorporate the multivalent effect into a PET probe design is through the conjugation of a multimeric targeting vector on a bifunctional chelator (BFC). For instance, dimeric, tetrameric and octameric forms of a cyclic-RGD (Arginine-Glycine-Aspartic Acid) peptide have been used to enhance the *in vivo* imaging properties of PET probes by the resulting multivalent effect.[26, 27]

Recently, we reported a BFC scaffold design, which provides a simple and effective way to impart multivalency to PET imaging probes labeled with ^{64}Cu.[28] This unique design of BFC scaffolds provides multiple peripheral functional points for multi-presentation of targeting vectors in a BFC without compromising the metal chelate stability of the chelating core. In

this work, we have extended this approach to NOTA-based radiopharmaceuticals by synthesizing a series of NOTA BFC scaffolds, $^{t}Bu_3$-**1**-COOH, $^{t}Bu_3$-**2**-$(COOH)_2$ and $^{t}Bu_3$-**3**-$(COOH)_3$. The NOTA BFC scaffold design maintains the intact Ga^{3+} chelating NOTA core (after ^{t}Bu deprotection) and varies the number of peripheral carboxylate groups from 1 – 3 to anchor the corresponding number of targeting molecules. This allows us to investigate the multivalent effect on ^{68}Ga-labeled PET probe design in a systematic way. In this study, a well-validated integrin $\alpha_v\beta_3$ ligand (c(RGDyK)) was used as a model targeting molecule to generate monovalent H_3**1**, divalent H_3**2**, and trivalent H_3**3** (Figure 3). For comparison, a monovalent analog (H_3**1a**) made from the commercial available NOTA-Bn-SCN was used as a positive control (Figure 3).[26]

Experimental Section

General Methods and Materials

All reactions were carried out under N_2 atmosphere in degassed dried solvents. Commercially available starting materials were purchased from commercial vendors and used directly without further purification unless otherwise stated. Milli-Q water (18 MΩ-cm) was obtained from a Millipore Gradient Milli-Q water system (Billerica, MA). All aqueous solutions were prepared with Milli-Q water. Silica gel 60 (70–230 mesh, Merck) was used for column chromatography. Analytical thin-layer chromatography (TLC) was performed using Merck 60 F254 silica gel (precoated sheets, 0.2 mm thick) (Lawrence, KS). The ^{1}H and ^{13}C NMR spectra were recorded on a Varian 400 or 500 MHz spectrometer; chemical shifts are expressed in ppm relative to TMS as reference peak (0.0 ppm). Matrix-assisted laser desorption/ionization (MALDI) mass spectra were acquired on an Applied Biosystems Voyager-6115 mass spectrometer. Radiolabeled conjugates were purified by Light C-18 Sep-Pak cartridges (Waters, Milford, MA). Radioactivity of tissue samples and radioactive standards were counted by an automated Gamma Counter, $Wizard_2$ 3″ (PerkinElmer).

Bulk solvents were removed by rotary evaporator under reduced pressure, and trace solvents were removed by vacuum pump. The α-Bromoglutaric acid-1-tertbutylester- 4-benzyl ester (**4)** was synthesized according to the published procedure.[29] The 1,4,7-triazacyclononane (TACN) and p-SCN-Bn-NOTA were purchase from Macrocyclics (Dallas, TX); and L-glutamic acid-5-benzylester was purchased from Sigma-Aldrich. The ^{68}Ge/^{68}Ga generator system was purchased from iThemba LABS (Somerset west, South Africa).

High Performance Liquid Chromatography (HPLC) Methods

HPLC separation was performed on a Waters 600 Multisolvent Delivery System equipped with a Waters 2996 Photodiode Array detector. The mobile phase consisted of H_2O with 0.1% TFA (solvent A) and acetonitrile with 0.1% TFA (solvent B). The analytical HPLC was performed on an XTerra RP18 column (150 × 4.6 mm) with a gradient of 0 % B to 100 % B in 50 min at a flow rate of 1.0 mL/min. The HPLC separation was performed on a semi-preparative XTerra RP18 Column (250 × 10 mm) with a gradient of 0% B to 100 % B in 50 min at a flow rate of 4.0 mL/min.

Integrin $\alpha_v\beta_3$ Receptor-Binding Assay

The $\alpha_v\beta_3$ integrin-binding affinities of c(RGDyK), H_3**1**, H_3**1a**, H_3**2**, and H_3**3** were determined by a competitive cell-binding assay using 125I-echistatin (PerkinElmer) as the $\alpha_v\beta_3$-specific radioligand. The experiments were performed on U87MG human glioblastoma cells following a previously reported method.[28] Briefly, U87MG cells were grown in RPMI 1640 medium supplemented with penicillin, streptomycin, and 10% (v/v) fetal bovine serum (FBS) at 37°C under 5% CO_2. Suspended U87MG cells in binding buffer (20 mM Tris, pH 7.4,150 mM NaCl, 2 mM $CaCl_2$, 1 mM $MgCl_2$, 1 mM $MnCl_2$, 0.1%

bovine serum albumin) were seeded on multi-well DV plates (Millipore) with 5×10^4 cells per well and then incubated with ^{125}I-echistatin (10,000 cpm/well) in the presence of increasing concentrations (0 – 5,000 nM) of c(RGDyK) peptide conjugates for 2 h. The final volume in each well was maintained at 200 μL. At the end of incubation, unbound ^{125}I-echistatin was removed by filtration followed by three rinses with cold binding buffer. The retentate was collected and the radioactivity was measured using a γ-counter. The best-fit IC_{50} values (inhibitory concentration where 50% of the ^{125}I-echistatin bound on U87MG cells are displaced) of c(RGDyK), H_3**1**, H_3**2**, and H_3**3** were calculated by fitting the data with nonlinear regression using GraphPad Prism (GraphPadSoftware, Inc.). Experiments were duplicated with quintuplicate samples.

Tissue Culture and Animal Model

All animal studies were performed in compliance with guidelines set by the UT Southwestern Institutional Animal Care and Use Committee (IACUC). The PC-3 cell line was obtained from the American Type Culture Collection (ATCC, Manassas, VA), and was cultured in T-media (Invitrogen, Carlsbad, CA) at 37 °C in an atmosphere of 5% CO_2 and were passaged at 75 % confluence in P150 plates. T-media was supplemented with 5% Fetal Bovine Serum (FBS) and 1 × Penicillin/Streptomycin. PC-3 cells were harvested from monolayer using PBS and trypsin/EDTA, and suspended in T-media with 5% FBS. The cell suspension was then injected subcutaneously (5×10^4 cells in 100 μL media) into the front left flanks of male SCID (Severe combined immunodeficiency) mice. After injection, animals were monitored three times a week by general observations. The tumor was allowed to grow three weeks to reach a palpable size (50 – 150 mm^3) for biodistribution and microPET-CT imaging studies.

Biodistribution

Male SCID mice bearing PC-3 prostate tumor xenograft were injected with 15–20 μCi of a ^{68}Ga labeled conjugate to evaluate the tissue distribution of the tracer in mice. All mice were sacrificed at 30 min and 2 h p.i. The organs of interest (tumor, blood, heart, lung, liver, spleen, kidneys, fat, bone, muscle, brain, small intestine, large intestine, and stomach) were harvested, weighed, and radioactivity was quantified using a γ-counter. Standards were prepared and counted along with the tissue samples to calculate the percent injected dose per gram (%ID/g) and percent injected dose per organ (%ID/organ). To determine the pharmacokinetic parameters, mice injected with the tracer were blood sampled from the retro-orbital sinus at 2, 5, 10, 30, 60, and 120 min. The pharmacokinetic parameters were calculated based on a two-compartment open model.[30] For in vivo stability evaluation, three SCID mice were used for each conjugate; each mouse was injected with 150 – 200 μCi of a ^{68}Ga labeled conjugate in 150 μL of saline *via* the tail vein. The mouse urine was collected within 2 h post injection (p.i.) and the lower part of the abdomen was pressed as necessary. The collected urine was filtered and analyzed by radio-HPLC.

Mouse PET/CT Imaging

The imaging studies were performed on a Siemens Inveon Multimodality PET/CT system (Siemens Medical Solutions Inc., Knoxville, TN, USA). Ten minutes prior to imaging, the animals were anesthetized using 3% isofluorane at room temperature until stable vitals were established. Once the animal was sedated, the animal was placed onto the imaging bed under 2% Isofluorane anesthesia for the duration of the imaging. The CT imaging was acquired at 80kV and 500 μA with a focal spot of 58 μm. The total rotation of the gantry was 360° with 360 rotation steps obtained at an exposure time of approximately 180 ms/frame. The images were attained using CCD readout of 4096 × 3098 with a binning factor of 4 and an average frame of 1. Under low magnification the effective pixel size was 103.03 μm. Total microCT scan time was approximately 6 minutes. The CT images were reconstructed with a down

sample factor of 2 using Cobra Reconstruction Software. The PET imaging was acquired directly following the acquisition of CT data. Each PC-3 tumor bearing mouse was injected with 100 – 125 μCi of a ^{68}Ga labeled conjugate in 100 μL of saline *via* tail vein. Immediately after the injection, a dynamic PET scan was performed from 0 – 30 min. The 0–30 min dynamic imaging data were reconstructed into six frames (5 min each frame), where each frame represented the average value of the respective 5 min interval. At 2 h p.i., a 15-min static scan was performed. PET images were reconstructed using Fourier Rebinning and Ordered Subsets Expectation Maximization 3D (OSEM3D) algorithm. Reconstructed CT and PET images were fused and analyzed using Inveon Research Workplace (IRW) software. For quantification, regions of interest were placed in the areas expressing the highest ^{68}Ga-labeled conjugate activity as determined by PET and guided by visual inspection of CT images. The tissues examined include the tumor, heart, liver, lung, kidney, and muscle. The resulting quantitative data were expressed in %ID/g.

Synthesis (Scheme 1)

Compound 5 and 6.[23]**:** A solution of α-bromoglutaric acid 1-tert-butyl ester 5-benzyl ester[29] (**4**, 0.40 g, 1.12 mmol) in 30 mL of chloroform was added over a period of 3 h to a solution of 1,4,7-triazacyclononane (**TACN**, 0.29 g, 2.24 mmol) in 40 mL of chloroform. The mixture was stirred over 3 d at room temperature and concentrated to give yellow oil. The crude product was purified by column chromatography (silica gel, $CHCl_3$/EtOH/NH_4OH 7:3:0.5) to give **5** (0.15 g, 50%) and **6** (40 mg, 15%) as colorless oil.

Compound 5: ^{1}H NMR ($CDCl_3$, 500 MHz) δ1.5 (s, 9H, $C(CH_3)_3$); 2.2–1.85 (m, 2H, $CHNCH_2$); 2.9–2.5 (m, 14H, NCH_2, $CH_2COOBzl$); 3.25 (dd, 1H, CHBr); 5.1 (s, 2H, CH_2Ph); 7.35 (m, 5H, Ph); MALDI-TOF/MS calcd for $C_{22}H_{35}N_3O_4$ $[M+H]^+$: 406.23. Found: 406.40.

Compound 6: ^{1}H NMR ($CDCl_3$, 500 MHz) δ1.4 (s, 18H, $C(CH_3)_3$); 1.9 (m, 2H); 2.05 (m, 2H); 2.45 (m, 2H); 2.55 (m, 2H); 2.8 (d, 2H); 3.0 (bs, 4H); 3.25 (m, 6H); 5.17 (s, 4H, CH_2Ph); 7.28 (m, 10H, Ph); MALDI-TOF/MS calcd for $C_{38}H_{55}N_3O_8$ $[M+H]^+$: 682.40. Found: 682.28.

Compound ^{t}Bu$_3$-1-Bn.[23]**:** The mixture of **5** (0.300 g, 0.740 mmol) and K_2CO_3 (0.20 g, 1.45 mmol) in 50 mL of anhydrous MeCN was cooled to 0 °C. To the above solution *t*-butyl-2-bromoacetate (0.26 g, 1.35 mmol) in 20 mL of anhydrous MeCN was added dropwise for 4 h. The reaction mixture was stirred at 0 °C for 6 h and at room temperature for 24 h. The mixture was filtered over Celite and the filtrate was evaporated to dryness. The crude product was purified by column chromatography (silica gel, CH_3Cl:EtOH 95:5) to provide *t*Bu$_3$-**1**-Bn as yellow oil (0.27 g, 57%). ^{1}H NMR ($CDCl_3$, 500 MHz) δ 1.5 (s, 27H, $C(CH_3)_3$); 1.85–3.6 (m, 21H, $CHNCH_2$, NCH_2, CH_2-COOBn, $CH_2COOtBu$); 5.1 (s, 2H, CH_2Ph); 7.35 (m, 5H, Ph); MALDI-TOF/MS calcd for $C_{34}H_{55}N_3O_8$ $[M+H]^+$: 635.40. Found: 635.75.

Compound ^{t}Bu$_3$-1-COOH.[23]**:** Compound ^{t}Bu$_3$-**1**-Bn (150 mg, 0.237 mmol) was dissolved in 20 mL of 2-propanol and the solution was degassed (N_2) for 5 min. To the above solution was added 10% Pd/C (50 mg) suspended in 0.5 mL of H_2O. The suspension was shaken in a hydrogenator (Parr, Moline, Illionis) at room temperature for 16 h under a H_2 atmosphere (60 psi). The suspension was filtered through Celite and the solvent was evaporated under vacuum. The obtained crude was purified by column chromatography (silica gel, 2-propanol/ammonia 95:5) to provide ^{t}Bu$_3$-**1**-COOH (85 mg, 66%) as yellow oil. ^{1}H NMR ($CDCl_3$, 500 MHz) δ1.5 (s, 27H, $C(CH_3)_3$); 2.0 (m, 2H); 2.5 (m, 2H); 2.8–3.2 (m, 12H);

3.45–3.75 (m, 5H); MALDI-TOF/MS calcd for $C_{27}H_{49}N_3O_8$ $[M+H]^+$: 544.35. Found: 544.68.

Compound $H_3$1: To a mixture of compound *t*Bu_3-**1**-COOH (5.0 mg, 9.0 μmol), *N*-hydroxysuccinimide (NHS, 10.0 mg, 88.7 μmol) and EDC·HCl (15.0 mg, 90.0 μmol) in 800 μL of anhydrous MeCN was added 20 μL of N, N-diisopropylethylamine (DIPEA). The mixture was then stirred under N_2 for 24 hours. After removal of the solvent under reduced pressure, the resulting residue was redissolved in $CHCl_3$ (1.0 mL) and then promptly washed with water (3 × 2 mL). The organic layer was evaporated, and the residue was dried by a lyophilizer to yield the NHS-activated ester as pale yellow solid (MALDI-TOF/MS calcd for $C_{31}H_{52}N_4O_{10}$ $[M+H]^+$: 641.37. Found: 641.42), The NHS-activated ester was used directly for the next step without further purification. Cyclic RGD peptide [c(RGDyK)] (7.0 mg, 11 μmol) was mixed with the NHS-activated ester in 500 μL of anhydrous DMF, to which 50 μL of DIPEA was added. The mixture was then stirred at room temperature for two days under N_2. After removal of the solvent, the crude product was purified by semi-preparative reverse-phase HPLC. The collected fractions of multiple runs were combined and lyophilized to afford 2.0 mg of *t*-butyl protected H_3**1** as white powder. MALDI-TOF/MS calcd for $C_{54}H_{88}N_{12}O_{15}$ $[M+H]^+$: 1144.65. Found: 1144.37. The *t*-butyl protected H_3**1** (2.0 mg, 1.74 μmol) was dissolved in 95% of TFA and stirred at room temperature for 12 h. After evaporation of the solvent, the residue was purified by semi-preparative reverse-phase HPLC. The collected fractions of multiple runs were pooled and lyophilized to afford H_3**1** as white solid in quantitative yield. MALDI-TOF/MS calcd for $C_{42}H_{64}N_{12}O_{15}$ ($[M+H]^+$: 976.46. Found: 976.43.

Compound ^{t}Bu$_3$-2-Bn$_2$: The mixture of **6** (85 mg, 0.12 mmol) and K_2CO_3 (86 mg, 0.62 mmol) in 40 ml of anhydrous MeCN was cooled to 0 °C. To the above solution *t*-butyl-2-bromoacetate (24 mg, 0.125 mmol) in 10 ml of anhydrous MeCN was added dropwise for 3 h. The reaction was stirred at 0 °C for 6 h and room temperature for 24 h. The mixture was filtered over Celite and the filtrate was evaporated to dryness. The crude product was purified by column chromatography (silica gel, $CHCl_3$/EtOH, 95: 5) to give *t*Bu_3-**2**-Bn_2 (80 mg, 80%) as yellow oil. ^{1}H NMR ($CDCl_3$, 500 MHz) δ 1.5–1.7 (s, 27H, $C(CH_3)_3$); 1.91–2.10 (m, 4H); 2.42–2.61 (m, 4H); 2.83 (bs, 3H); 3.1 (bs, 5H); 3.3 (bs, 3H); 3.5 (bs, 2H); 3.80–4.14 (m, 3H); 5.1 (s, 4H, CH_2Ph); 7.25 (m, 10H, Ph); ^{13} 25.20, 28.16, 31.05, 53.38, 55.28, 58.59, 64.46, C NMR ($CDCl_3$,100 MHz) δ77.00, 80.90, 81.97, 85.21, 126.79, 128.08, 135.92, 171.99, 172.87. MALDI-TOF/MS calcd for $C_{44}H_{65}N_3O_{10}$ $[M+H]^+$: 796.47. Found: 796.67.

Compound ^{t}Bu$_3$-2-(COOH)$_2$: Compound *t*Bu_3-**2**-Bn_2 (50 mg, 0.15 mmol) was dissolved in 20 mL of 2-propanol and the solution was degassed (N_2) for 5 min. To the above solution was added 10% Pd/C (30 mg) suspended in 0.5 mL of H_2O. The suspension was shaken in a hydrogenator (Parr, Moline, Illionis) at room temperature for 16 h under a H_2 atmosphere (60 psi). The suspension was filtered through Celite and the solvent was evaporated under vacuum. The obtained crude was purified by column chromatography (silica gel, 2-propanol/ammonia 95:5) to provide ^{t}Bu_3-**2**-$(COOH)_2$ (30 mg, 66%) as yellow oil. ^{1}H NMR ($CDCl_3$, 500 MHz) δ1.6 (s, 27H, $C(CH_3)_3$); 2.4–2.8 (m, 7H); 3.0–3.3 (m, 12H); 3.45–3.75 (m, 5H); MALDI-TOF/MS calcd for $C_{30}H_{53}N_3O_{10}$ $[M+H]^+$: 615.37. Found: 615.56.

Compound $H_3$2: To a mixture of compound *t*Bu_3-**2**-$(COOH)_2$ (5.0 mg, 8.5 μmol), *N*-hydroxysuccinimide (10.0 mg, 80.0 μmol) and EDC·HCl (10.5 mg, 55.0 μmol) in 500 μL of dry MeCN was added 20 μL of N, N-diisopropylethylamine (DIPEA), which was then stirred under N_2 for 24 hours. Solvent was removed under reduced pressure, the residue was redissolved in $CHCl_3$ (1 mL) and then promptly washed with water (3 × 2 mL). The $CHCl_3$ was evaporated, the residue was dried by a lyophilizer to yield NHS-activated ester as pale

yellow solid (MALDI-TOF/MS calcd for $C_{38}H_{59}N_5O_{14}$ $[M+H]^+$: 808.41. Found: 808.18), NHS-activated ester was used directly for the next step without further purification. Cyclic RGD peptide [c(RGDyK)] (10.5 mg, 17 μmol) was mixed with the above yellow solid in 500 μL of anhydrous DMF, to which 50 μL of DIPEA was added. The mixture was then stirred at room temperature for two days under N_2. After evaporation of the solvent under vacuum, the crude product was purified by a semi-preparative reverse-phase HPLC. The collected fractions of multiple runs were combined and lyophilized to afford t-butyl protected H_3**2** as white powder. MALDI-TOF/MS calcd for $C_{84}H_{131}N_{21}O_{24}$ $[M+H]^+$: 1818.97. Found: 1818.74. The *t*-butyl protected H_3**2** (3.5 mg, 1.9 μmol) was dissolved in 95% of TFA and stirred at room temperature for 12 h. After evaporation of the solvent, the residue was purified by semi-preparative reverse-phase HPLC. The collected fractions of multiple runs were pooled and lyophilized to afford a white solid H_3**2** in quantitative yield. MALDI-TOF/MS calcd for $C_{72}H_{107}N_{21}O_{24}$ ($[M+H]^+$: 1649.78. Found: 1649.38.

Compound ^{t}Bu$_3$-3-Bn$_3$: To a suspension of **TACN** (68 mg, 0.525 mmol) and K_2CO_3 (1.2 g, 8.68 mmol) in 3 mL of anhydrous MeCN at room temperature, compound **4** (620 mg, 1.74 mmol) in 3 mL of anhydrous MeCN was added dropwise. After the addition, the reaction was allowed to proceed at room temperature for 24 h and then at 55 °C for 24 h. The solids were removed by filtration and washed with chloroform (2 × 20 mL). The combined filtrate was concentrated under vacuum and purified by column chromatography (silica gel, 60- 230 mesh) using using $CHCl_3$ to EtOAc for elution. Compound ^{t}Bu$_3$-**3**-Bn$_3$ was obtained as a sticky oil (350mg; Yield, 70%): ^{1}H NMR ($CDCl_3$, 400 MHz) δ 1.42 (s, 27H), 1.76–1.88 (m, 3H), 1.90–2.04 (m, 3H), 2.38–2.58 (m, 8H), 2.64–2.84 (m, 8H), 2.86–2.96 (m, 2H), 3.04–3.14 (m, 3H), 5.08 (s, 6H), 7.32 (s, 15H); ^{13}C NMR ($CDCl_3$, 100 MHz) δ 25.63, 28.55, 31.31, 52.61–54.42 (br), 66.42, 67.22, 81.08, 128.41, 128.47, 128.77, 136.28, 172.74, 173.47. MALDI-TOF/MS calcd for $C_{54}H_{75}N_3O_{12}$ $[M+H]^+$: 958.54. Found: 958.77. Anal. Calcd for $C_{54}H_{75}N_3O_{12}\cdot H_2O$: C, 66.44; H, 7.95; N, 4.30. Found: C, 66.41; H, 7.65; N, 4.30.

Compound ^{t}Bu$_3$-3-(COOH)$_3$: To a solution of ^{t}Bu$_3$-**3**-Bn$_3$ (100 mg, 0.128 mmol) in 5 mL of 2-propanol was added portion wise 10 mg of 10% Pd/C. The suspension was shaken in a hydrogenator (Parr, Moline, Illionis) at room temperature for 16 h under a H_2 atmosphere (60 psi). After removal of the solids, evaporation of solvent under vacuum gave the target compound ^{t}Bu$_3$-**3**-(COOH)$_3$ as white solid in nearly quantitative yield. ^{1}H NMR ($CDCl_3$, 400 MHz) δ 1.48 (s, 27H), 2.07 (br, 6H), 2.50 (br, 8H), 3.15 (br, 10H), 3.62 (br, 3H), 8.35 (br. 3H); ^{13}C NMR (CD_3OD, 100 MHz) δ 25.16, 27.34, 31.27, 45.55, 63.39, 82.89, 171.41, 15.24; MALDI-TOF/MS calcd for $C_{33}H_{57}N_3O_{12}$ $[M+H]^+$: 687.39. Found: 688.89. Anal. Calcd for $C_{33}H_{54}N_3Na_3O_{12}$: C, 52.58; H, 7.22; N, 5.57. Found: C, 52.58; H, 7.22; N, 5.59.

Compound $H_3$3: To a mixture of compound *t*Bu$_3$-**3**-(COOH)$_3$ (3.8 mg, 5.5 μmol), *N*-hydroxysuccinimide (6.2 mg, 55.0 μmol) and EDC HCl (10.5 mg, 55.0 μmol) in 500 μL of dry MeCN was added 20 μL of N, N-diisopropylethylamine (DIPEA), which was then stirred under N_2 for 24 hours. After the solvent was removed under reduced pressure, the residue was redissolved in $CHCl_3$ (1 mL) and then washed 3 times (3 × 2 mL) with water promptly. The organic layer was evaporated to remove $CHCl_3$, the resulting residue was then dried by a lyophilizer to NHS-activated ester as pale yellow solid (MALDI-TOF/MS calcd for $C_{45}H_{60}N_6O_{18}$ $[M+H]^+$: 979.44. Found: 979.40), NHS-activated ester was used directly for the next reaction without further purification. Cyclic RGD peptide [c(RGDyK)] (10.5 mg, 17 μmol) was mixed with the above yellow solid in 500 μL of anhydrous DMF, to which 50 μL of DIPEA was added. The mixture was then stirred at room temperature for two days under N_2. After evaporation of the solvent under vacuum, the crude product was purified by a semi-preparative reverse-phase HPLC. The collected fractions of multiple runs were combined and lyophilized to afford 4.5 mg of t-butyl protected H_3**3** as white powder

(33%). MALDI-TOF/MS calcd for $C_{114}H_{174}N_{30}O_{33}$ $[M+H]^+$: 2490.29. Found: 2490.21. The *t*-butyl protected H_3**3** (2.0 mg, 0.80 μmol) was dissolved in 95% of TFA and stirred at room temperature for 12 h. After evaporation of the solvent, the residue was purified by semi-preparative reverse-phase HPLC. The collected fractions of multiple runs were pooled and lyophilized to afford a white solid H_3**3** in quantitative yield. MALDI-TOF/MS calcd for $C_{102}H_{150}N_{30}O_{33}$ $[M+H]^+$: 2321.10. Found: 2321.43.

Compound $H_3$1a: To a solution of *p*-SCN-Bn-NOTA (10 mg, 22 μmol) in 200 μL of anhydrous DMF was added a mixture of [c(RGDyK)] (3.3 mg, 5 μmol) and DIPEA (20 μL) in 200 μL of anhydrous DMF. The mixture was then stirred at room temperature for 24 h. After evaporation of the solvent, the residue was purified by semi-preparative reverse-phase HPLC. The collected fractions from multiple runs were pooled and lyophilized to afford 5.0 mg of H_3**1a** as white solid (88%). MALDI-TOF/MS calcd for $C_{47}H_{67}N_{13}O_{14}$ $[M+H]^+$: 1070.47. Found: 1070.48.

Radiolabeling of $H_3$1, $H_3$1a, $H_3$2, and $H_3$3 with ^{68}Ga: To a 2.0 mL vial containing 5–10 μg of respective conjugate in 1400 μL of 1 M 4-(2-hydroxyethyl)-1-piperazineethanesulfonic acid (HEPES, pH = 6.5) solution, 2 – 3 mCi of $^{68}GaCl_3$ in 0.6 N HCl was added. The reaction mixture was shaken and incubated at 75°C for 0.5 h. Then, 2 μL of 5 mM ethylendiaminetetraacetic acid (EDTA) was added to the reaction mixture, which was allowed to incubate for another 5 min (EDTA was used to remove non-specifically bound or free ^{68}Ga from the ^{68}Ga-labeled conjugate). The purification of ^{68}Ga-labeled conjugate was carried out by passing the mixture through a preconditioned Sep-Pak C-18 light cartridge. After thorough rinsing (3 × 3 mL, water) of the cartridge, the ^{68}Ga -labeled conjugate was eluted by an ethanol-water mixture (70:30). The product was first analyzed by a Rita Star Radioisotope TLC Analyzer (Straubenhardt, Germany) on instant thin-layer chromatography (ITLC-SG) plates (Pall Life Sciences, East Hills, NY) and then by radio-HPLC to determine the radiochemical purity of the product.

Statistical Analysis

Quantitative data were expressed as the mean ± SD. Unpaired *t* test (two-tailed, confidence intervals: 95%) was performed using GraphPad Prism. *P* values of <0.05 were considered statistically significant.

Results

Synthesis

The synthesis of H_3**1**, H_3**2** and H_3**3** ^{t}Bu$_3$-**1**-COOH, *t*Bu$_3$-**2**-(COOH)$_2$ and ^{t}Bu$_3$-**3**-(COOH)$_3$; second, conjugation of c(RGDyK) with ^{t}Bu$_3$-**1**-COOH, *t*Bu$_3$-**2**-(COOH)$_2$ and ^{t}Bu$_3$-**3**-(COOH)$_3$, followed by the deprotection of the *t*-butyl protected carboxylate groups. The side-arm, α-bromoglutaric acid-1-tertbutylester-4-benzyl ester **4** was synthesized by two steps from commercially available L-glutamic acid-5-benzylester.[29] Alkylation of the commercially available **TACN** with **4** in $CHCl_3$ at room temperature gave both mono- (**5**, 50%) and di-alkylated (**6**, 15%) products. Compounds **5** and **6** were separated using column chromatography, where compound **6** was eluted first. Further alkylation of **5** and **6** with bromo-*t*-butylester afforded ^{t}Bu$_3$-**1**-Bn (57%) and *t*Bu$_3$-**2**-Bn$_2$ (80%), respectively. Over-alkylation was observed during the reaction between **5** or **6** with bromo-*t*-butylester, which led to the respective quaternary ammonium salt. However, the salt formation was avoided by slow addition of bromo-*t*-butylester to the diluted solution of **5** or **6**. Alkylation of **TACN** with **4** (3.3 equivalents) afforded *t*Bu$_3$-**3**-Bn$_3$ in a yield of over 70% without formation of mono- or di-substituted analogs under the given reaction conditions.

The protected BFC scaffolds, $^{t}Bu_3$-**1**-Bn, *t*Bu_3-**2**-Bn_2 and *t*Bu_3-**3**-Bn_3, contains two protected carboxylate groups at α and γ positions of the side-arm. The benzyl protected γ-carboxylate groups in $^{t}Bu_3$-**1**-Bn, *t*Bu_3-**2**-Bn_2 and *t*Bu_3-**3**-Bn_3 were selectively deprotected and reserved for peptide (c(RGDyK)) conjugation. Catalytic debenzylation of $^{t}Bu_3$-**1**-Bn, *t*Bu_3-**2**-Bn_2 and $^{t}Bu_3$-**3**-Bn_3 was achieved using 10% Pd/C in 2-propanol under hydrogen atmosphere to afford $^{t}Bu_3$-**1**-COOH, *t*Bu_3-**2**-$(COOH)_2$ and $^{t}Bu_3$-**3**-$(COOH)_3$ in quantitative yield. The obtained γ-carboxylic acids were then activated by N-hydroxysuccinimide (NHS) for acid-amine conjugation chemistry and used as received for further conjugation. The conjugation of NHS-activated $^{t}Bu_3$-**1**-COOH, *t*Bu_3-**2**-$(COOH)_2$ and $^{t}Bu_3$-**3**-$(COOH)_3$ with 1 – 3 equivalents of c(RGDyK) in the presence of DIPEA provided the *t*-butyl protected conjugates in 30 – 45 % yields. Finally, the α-carboxylate group was deprotected using 95% trifluoroacetic acid to provide H_3**1,** H_3**2,** and H_3**3,** each containing three internal carboxylic acids for ^{68}Ga labeling. The H_3**1a** conjugate was prepared by directly reacting *p*-SCN-Bn-NOTA with c(RGDyK) peptide at room temperature in aqueous media using a reported procedure.[15, 26]

All the intermediates and final products were characterized by ^{1}H NMR, mass spectroscopy and HPLC. Analysis of ^{1}H NMR spectra was facilitated by addition or removal of characteristic *t*-butyl and/or benzyl groups. Also, these compounds were characterized by their molecular ion peak by MALDI-mass spectrometry, and the purity of these conjugates was assured by observing a single peak in the reverse-phase HPLC.

Radiochemistry

The ^{68}Ga labeling efficiencies were evaluated under an acidic condition (pH = 3.0 – 3.5)[31] for all the conjugates by varying the reaction temperature and time. At room temperature, conjugates H_3**1,** and H_3**1a** showed a high ^{68}Ga incorporation rate (> 90%) within 10 min of the radiochemical reaction, while H_3**2** and H_3**3** only had 71% and 84%, respectively. When the reaction proceeded to 30-min, all the conjugates were radiolabeled with > 95% of ^{68}Ga. At 70°C, all conjugates showed nearly instant labeling with ^{68}Ga. The ^{68}Ga labeled conjugates were purified in one step using a pre-activated C-18 Sep-Pak light cartridge with a > 90% recovery rate. The radiochemical purity of the ^{68}Ga-labeled conjugates after cartridge purification was > 99% as determined by radio-HPLC. The overall radiochemical procedure including the purification and HPLC steps took less than 45 min and gave a decay-corrected radiochemical yield of > 90%. The specific activity of the purified ^{68}Ga-labeled conjugates was in the range of 33 – 44 MBq/nmol. The ^{68}Ga-labeled conjugates were eluted from HPLC less than one min earlier than their respective conjugate.

Cell-binding assay

The *in vitro* $\alpha_v\beta_3$ binding affinities of c(RGDyK), H_3**1**, H_3**2**, and H_3**3** were determined by a competitive cell-binding assay using ^{125}I-echistatin as the integrin-specific radioligand.[32] The receptor binding experiments were performed using $\alpha_v\beta_3$ integrin-positive U87MG human glioma cells containing a high $\alpha_v\beta_3$ integrin density on its cell surface.[33] All the conjugates inhibited the binding of ^{125}I-echistatin to the $\alpha_v\beta_3$ integrin-positive U87MG cells in a dose-dependent manner (Figure S1). Calculated IC_{50} values expressed by the 50% inhibitory concentration of the ^{125}I-echistatin binding were 204 ± 76 nM (c(RGDyK)), 218 nM (H_3**1a**),[26] 171 ± 60 nM (H_3**1**), 43.9 ± 16.1 nM (H_3**2**) and 14.7 ± 5.0 nM (H_3**3**). The *in vitro* $\alpha_v\beta_3$ binding affinity of c(RGDyK) was used as a reference. The binding affinity of H_3**1** is similar to that of c(RGDyK), indicating that the conjugation of a NOTA scaffold to c(RGDyK) had minimal effect on the receptor binding affinity of c(RGDyK). The multivalent enhancement ratio (MVE) calculated by dividing the IC_{50} value of H_3**1** by that of H_3**2** or H_3**3** and the respective number of c(RGDyK) molecules, was 3.9 for H_3**2** and 11.6 for H_3**3**, indicative of the anticipated multivalent effect.[28, 34]

In vivo stability

The metabolic stability of ^{68}Ga-**1**, ^{68}Ga-**1a**, ^{68}Ga-**2** and ^{68}Ga-**3** in SCID mice was evaluated by examining their metabolites in urine at 2 h p.i. Impressively, no metabolites were detected for any of the conjugates by radio-HPLC analysis (Figure S2), indicating high *in vivo* stability of ^{68}Ga-labeled conjugates.

Biodistribution

The pharmacokinetics (PK) parameters for ^{68}Ga-**1**, ^{68}Ga-**1a**, ^{68}Ga-**2**, and ^{68}Ga-**3** were evaluated in SCID mice using a two-compartment open model. The time-activity curves of the ^{68}Ga-labeled conjugates in blood showed a biphasic clearance (Figure 4). As shown in Table 1, all the ^{68}Ga-labeled conjugates displayed a rapid distribution half-life ($t_{1/2(\alpha)} < 5$ min) and a short terminal half-life ($t_{1/2(\beta)} < 50$ min).

The tissue distribution profiles of ^{68}Ga-**1**, ^{68}Ga-**1a**, ^{68}Ga-**2** and ^{68}Ga-**3** in SCID mice bearing the $\alpha_v\beta_3$ integrin-positive PC-3 tumor are summarized in Figure 5 and Table S3. Among the organs evaluated, kidney showed the highest uptake (^{68}Ga-**1a**: 6.25 ± 0.61 %ID/g; ^{68}Ga-**1**: 5.40 ± 0.61 %ID/g; ^{68}Ga-**2**: 3.18 ± 2.76 %ID/g; ^{68}Ga-**3**: 8.41 ± 0.99 %ID/g) at 30 min p.i., indicating that all the conjugates were primarily excreted through the renal route. At 2 h p.i., less than 60% of the kidney uptake was retained for monovalent conjugates (^{68}Ga-**1a**: 2.95 ± 0.76 %ID/g; ^{68}Ga-**1**: 3.14 ± 0.13 %ID/g), while the divalent and trivalent ones showed a > 90% retention (^{68}Ga-**2**:3.86 ± 1.80 %ID/g; ^{68}Ga-**3**: 7.50 ± 0.95 %ID/g). At 30 min p.i., no significant difference was observed for the liver uptake of the conjugates (^{68}Ga-**1a**: 1.98 ± 0.29 %ID/g; ^{68}Ga-**1**: 1.91 ± 0.30 %ID/g; ^{68}Ga-**2**: 2.07 ± 0.05 %ID/g; ^{68}Ga-**3**: 3.10 ± 0.77 %ID/g). Interestingly, the liver uptake retention was independent of the valency of the conjugates at 2 h p.i. However, the tumor uptake of the conjugates showed a positive correlation with the valency (^{68}Ga-**1a**: 1.63 ± 0.19 %ID/g; ^{68}Ga-**1**: 1.67 ± 0.16 %ID/g; ^{68}Ga-**2**: 1.94 ± 0.32 %ID/g; ^{68}Ga-**3**: 4.41±1.00 %ID/g) at 2 h p.i., which clearly reflects the multivalent effect and is consistent with the cell binding affinities of the conjugates. Impressively, the tumor retention rate of the uptake shown at 2 h p.i. was in the order of trivalent ^{68}Ga-**3** (79%) > divalent ^{68}Ga-**2** (61%) > monovalent ^{68}Ga-**1** (55%) monovalent ^{68}Ga-**1a** (57%) at 2 h p.i.

Mouse PET-CT Imaging

The PET-CT imaging was performed on SCID mice bearing integrin $\alpha_v\beta_3$-positive PC-3 prostate cancer xenograft. Representative decay-corrected coronal images at 30 min (dynamic frame of 25 – 30 min) and 2 h p.i. are shown in Figure 6a. The PC-3 tumors were clearly visualized by all four probes at 30 min p.i. but without significant tumor uptake difference observed among the conjugates (^{68}Ga-**1a:** 3.24 ± 0.41 %ID/g; ^{68}Ga-**1**: 3.26 ± 0.70 %ID/g; ^{68}Ga-**2**; 3.06 ± 0.21 %ID/g; and ^{68}Ga-**3**: 3.55 ± 0.85 %ID/g) (Table S1). Uptake of ^{68}Ga-**1**, ^{68}Ga-**1a**, ^{68}Ga-**2** and ^{68}Ga-**3** at 30 min p.i. in other organs, especially muscle and blood, was also high, which resulted in the low tumor-to-background contrast. At 2 h p.i., the tumor-to-background contrast clearly increased as the ^{68}Ga-labeled conjugate was cleared from the non-target organs (Figure 6d). Of the ^{68}Ga-labeled conjugates, ^{68}Ga-**3** showed the highest tumor uptake at 2 h p.i. (2.55 ± 0.50 %ID/g), which is significantly ($p < 0.05$) higher than all other ^{68}Ga-labeled conjugates (^{68}Ga-**2**: 1.90 ± 0.10 %ID/g; ^{68}Ga-**1**: 1.66 ± 0.15 %ID/g; and ^{68}Ga-**1a**:1.40 ± 0.36 %ID/g) (Figure 6c). This observation can be explained by the enhanced binding affinity of the trivalent ^{68}Ga-**3** conjugate, which led to its prolonged retention in the target, integrin $\alpha_v\beta_3$-positive tumor. Compared to the corresponding 30-min uptake value, the tumor uptake retention at 2 h p.i. follows the same order as observed in the biodistribution result: trivalent ^{68}Ga-**3** (72%) > divalent ^{68}Ga-**2** (62%) > monovalent ^{68}Ga-**1** (51%) ~ monovalent ^{68}Ga-**1a** (43%). A blockade experiment was performed by co-injecting the ^{68}Ga-labeled conjugate with the blocking dose of

c(RGDyK) (10 mg/kg). The drastic reduction of tumor uptake for all ^{68}Ga-labeled conjugates unequivocally indicated their imaging specificity of integrin $\alpha_v\beta_3$ (Table S1).

Consistent with the biodistribution data, all ^{68}Ga-labeled conjugates showed efficient clearance from the kidney (Table S1). Possibly due to the multivalent effect, ^{68}Ga-**3** showed the highest kidney uptake (4.03 ± 1.75 %ID/g) at 2 h p.i., which is significantly higher than other ^{68}Ga-labeled conjugates ($p < 0.01$) (Figure 6b, Table S1). In the liver, no significant uptake and retention difference was observed for the ^{68}Ga-labeled conjugates at either 30 min or 2 h p.i. Low to negligible level (< 1.14 %ID/g) of uptake was observed in other major organs (e.g. heart, lungs, muscle) at 2 h p.i.

Discussion

The design of a BFC for metal-based radiopharmaceuticals is largely influenced by the ability of the BFC to form a kinetically inert chelate with a metal radionuclide and the ease to covalently anchor a targeting vector. To date, both cyclic and acyclic BFCs containing coordinating atoms (e.g. nitrogen, oxygen and sulfur) have been reported for Ga(III) chelation.[35–38] For a BFC to be considered for nuclear imaging probe design, its complex with the metal ion of interest must have desirable thermodynamic and *in vivo* kinetic stability, specifically resistance to trans-metalation with serum proteins. The most commonly used macrocyclic chelator, 1, 4, 7, 10-tetraazacyclododecanetetraacetic acid (DOTA), is a choice of convenience for ^{68}Ga PET imaging design due to its commercial availability and the fact that it is in the composition of several FDA-approved agents. However, the DOTA complex with Ga(III) has a thermodynamic stability constant (log K = 21.33)[39] comparable to that of the transferrin complex with Fe(III) (log K = 20.3),[40] which may lead to in vivo transmetalation.[40] Also, the complexation kinetics of DOTA with Ga(III) often require an elevated temperature and a long reaction time, which could be detrimental to the activity of the biomolecule and not advantageous to ^{68}Ga, a radionuclide with a decay half-life barely longer than one hour. Given the small ionic radius of Ga(III) (76 pm),[18] NOTA, a nine-membered triazamacrocyclic chelator, would provide a perfect cavity size match for Ga(III) coordination. Indeed, the thermodynamic stability constant of Ga(III)-NOTA complex (log K = 30.98)[22, 24] is approximately 10 orders of magnitude higher than that of its DOTA counterpart. More impressively, the neutral Ga(III)-NOTA complex was reported to stay inert against the acid-catalyzed dissociation in 6N HNO_3 for 6 days.[20] When NOTA is used without modification as a BFC, however, one of its three pendent coordinating carboxylic acids would be consumed to form an amide linkage with the targeting vector. Although the coordinating atoms (N_3O_3) stay the same before and after the conjugation, the stability of the metal complex moiety is compromised due to the formation of an amide linkage.[41, 42] In order for NOTA to keep its three coordinating acetate arms intact for Ga(III) chelation, an additional functional group is necessary. Indeed, various C- or N-functionalized NOTA derivatives have been reported as modified NOTA for gallium radiopharmaceuticals.[23, 43–46] Of the reported methods, the N-functionalization of TACN provides a simple and versatile way of introducing additional functionalities to the triazamacrocyclic ring, which makes the NOTA derivatives bifunctional.[23, 24]

The multivalent effect is widely used to enhance the desired biological potency of a bioactive molecule.[47–50] For instance, the tumor targeting efficacy of a targeting vector can be enhanced by orders of magnitude through the strengthened specific ligand-receptor binding.[28, 34, 51–54] In principle, multimeric presentation of a ligand increases its local concentration on the cell surface thus increasing the probability of the specific ligand-receptor interaction, which results in enhanced target accumulation. Furthermore, the juxtaposition of the conjoined ligands can facilitate the desired ligand-receptor interaction. In the field of molecular imaging, multivalent effect can certainly be exploited to amplify

the imaging signal in target organs or tissues in the same manner. Indeed, several groups have reported that imaging contrast can be significantly improved by taking advantage of multivalent effect in the imaging probe design.[27, 28, 32, 55–58] For instance, multivalent PET imaging probes featuring multimeric peptides have demonstrated better imaging properties than their monomeric counterpart.[32, 55, 59–64]

Recently, we reported a BFC scaffold design for ^{64}Cu-based PET imaging probes, which provides multiple peripheral functional points for multi-presentation of targeting vectors in a BFC without compromising the metal chelate stability of the chelating core.[28] An important role of such a BFC scaffold is to provide PET signal enhancement through the resulted multivalent effect. Similarly, we designed a series of NOTA-based scaffolds for ^{68}Ga PET imaging probes, ^{t}Bu$_3$-**1**-Bn,23 ^{t}Bu$_3$-**2**-Bn$_2$ and ^{t}Bu$_3$-**3**-Bn$_3$, which contain two orthogonally protected carboxylic acid groups on each side-arm. All three BFC scaffolds have three *t*-butyl protected α-carboxylic acid groups intended for Ga(III) coordination, while the number of the terminal benzyl protected γ-carboxylic acid differs to systematically vary the valency of a targeting vector from 1 – 3. The orthogonality of the protecting groups on the side-arm enables the selective deprotection of the γcarboxylate and α-carboxylate groups by different procedures at the corresponding step. Further, the four-carbon alkyl chain is incorporated as a spacer between the NOTA core and the peripheral carboxylate groups so as to minimize the interference of the NOTA motif with the properties of the targeting vector. Indeed it was reported that replacing one of the acetic acid side arms of NOTA with succinic acid, a 4-carbon spacer, has a negligible effect on the geometry or the thermodynamic stability of the resulting Ga(III) complex (Ga-NODASA: log K = 30.9; Ga-NOTA: log K = 30.98).[24] Impressively, the exchange kinetics of ^{67}Ga-NODASA with transferrin at the physiological pH and temperature showed no metal transchelation over the period of 5 days.[24] Therefore, we believe the replacement of the acetate side-arm with α-bromoglutaric acid 1-tert-butyl ester 5-benzyl ester (**4**) would not adversely influence the structural integrity and thermodynamic stability of the resulting Ga-complexes.

The NOTA BFC scaffolds, ^{t}Bu$_3$-**1**-COOH, *t*Bu$_3$-**2**-(COOH)$_2$ and ^{t}Bu$_3$-**3**-(COOH)$_3$, were synthesized by alkylation of TACN using appropriate equivalents of **4.** Synthesis of ^{t}Bu$_3$-**1**-COOH and ^{t}Bu$_3$-**2**-(COOH)$_2$ was performed in a three-step route with the first step determining the overall yield. The alkylation of TACN with **4** afforded both **5** and **6**. The subsequent two steps were quantitative. Synthesis of ^{t}Bu$_3$-**3**-(COOH)$_3$ was straightforward, which can be scaled to produce grams of the product. The NOTA scaffolds (^{t}Bu$_3$-**1**-COOH, *t*Bu$_3$-**2**-(COOH)$_2$ and ^{t}Bu$_3$-**3**-(COOH)$_3$) possess one, two and three peripheral catboxylate groups, respectively, for the covalent attachment of a targeting vector in a systematic fashion. For proof of concept, a well-validated integrin $\alpha_v\beta_3$ ligand, c(RGDyK), was conjugated to ^{t}Bu$_3$-**1**-COOH, *t*Bu$_3$-**2**-(COOH)$_2$ and ^{t}Bu$_3$-**3**-(COOH)$_3$ to yield ^{t}Bu-protected monvalent, divalent, and trivalent peptide conjugates. The ^{t}Bu-protected α-carboxylate was later deprotected in 95% TFA to give H$_3$**1,** H$_3$**2,** and H$_3$**3** in quantitative yield as peptide conjugates ready for labeling with ^{68}Ga.

Radiolabeling of the conjugates of H$_3$**1,** H$_3$**2,** and H$_3$**3** with ^{68}Ga was tested by varying reaction conditions, such as pH, temperature, and time, in order to reach the highest achievable specific activity of the labeled tracers within a short time, given the 68-min half-life of ^{68}Ga. Because radiolabeling of NOTA with ^{68}Ga is pH sensitive, HEPES was used as the reaction buffer to provide the optimal labeling pH (3.0 – 3.5).[16] At room temperature, we were able to label the conjugates in high radiochemical yields (RCY > 95%) within 30 min. Comparatively speaking, the ^{68}Ga labeling of multivalent conjugates (H$_3$**2,** and H$_3$**3**) was slower than that of the monvalent ones (H$_3$**1** and H$_3$**1a**) in part due to the steric hindrance by the additional copies of c(RGDyK) peptide. However, the difference virtually disappeared when the radiolabeling was conducted at 70°C. One of the desired features of a

PET imaging agent for clinical application is the ease of post-labeling purification. By a simple separation procedure through a C-18 cartridge, all the radiolabeled conjugates reached > 99% radiochemical purity as determined by radio-HPLC.

Both H_3**1** and H_3**1a** have one copy of c(RGDyK) peptide while H_3**2** and H_3**3** have two and three copies of c(RGDyK), respectively. The multi-presentation of the c(RGDyK) peptide in H_3**2** and H_3**3** is expected to enhance the affinity of the receptor-ligand interaction through the phenomenon of multivalent effect. By a competitive cell-binding assay using ^{125}I-echistatin as the integrin-specific radioligand,[32] multivalent effect, as measured by the enhanced specific ligand-receptor binding affinity was evaluated. The determined IC_{50} values of monvalent H_3**1** (171 ± 60 nM), divalent H_3**2** (43.9 ± 16.1 nM), and trivalent H_3**3** (14.7 ± 5.0 nM) were found to be similar to the measurements reported for the monovalent (H_3**1a**, 218 nM), divalent (60 nM) and tetravalent (16 nM) conjugates constructed from peptide multimerization of c(RGDyK).[26] The cell-binding assay clearly demonstrated the anticipated multivalent effect of H_3**2** and H_3**3** as compared to their monovalent counterpart (H_3**1**). Of note, the multivalent effect resulted from the BFC scaffold-based multivalency (H_3**3**, 13 nM) is similar to that resulted from the tetramerization of c(RGDyK) (NOTA-Bn-SCN–tetramer, 16 nM).[26]

The *in vivo* behavior of ^{68}Ga-**1**, ^{68}Ga-**1a**, ^{68}Ga-**2** and ^{68}Ga-**3**, was evaluated in SCID mice bearing integrin $\alpha_v\beta_3$-positive PC-3 prostate cancer xenograft. Like other c(RGDyK) based agents, all the ^{68}Ga-labeled conjugates were efficiently cleared from the kidneys, while the excretion through feces was negligible within 2 h p.i. The radio- HPLC analysis of collected urine demonstrated that the ^{68}Ga-labeled conjugates stayed intact (> 99%) within 2 h p.i, which is roughly two times of the physical half-life of ^{68}Ga. This high metabolic stability of the ^{68}Ga-labeled conjugates likely resulted from the kinetic inertness of the Ga-NOTA complex.

The integrin $\alpha_v\beta_3$ positive PC-3 tumor was visualized with ^{68}Ga-**1**, ^{68}Ga-**1a**, ^{68}Ga-**2,** and ^{68}Ga-**3** at 30 min and 2 h p.i. (Figure 6a). Irrespective of the valency, all the ^{68}Ga-labeled conjugates showed similar tumor uptake with poor contrast at 30 min p.i. due to their relatively high level of presence in the non-target organs (e.g. blood and muscle. Table S3). At 2 h p.i., the enhanced tumor uptake and retention of ^{68}Ga-**2** and ^{68}GA-**3** can be partially attributed to their increased binding affinities resulting from multivalent effect. Interestingly, the tumor PET signal amplification level by the multivalent effect (^{68}Ga-**3**: 2.55 ± 0.50 %ID/g; ^{68}Ga-**2:** 1.90 ± 0.10 %ID/g; ^{68}Ga-**1**: 1.66 ± 0.15 %ID/g) is similar to that in a published work using peptide multimerization of c(RGDyK) as an approach to realize multivalent effect for PET probe design (tetramer: 2.1 %ID/g; dimer: 1.9 %ID/g; monomer: 1.1 %ID/g).[26] In addition to the increased binding affinity, the prolonged *in vivo* half-life of multivalent conjugates, resulting from the molecule size increase, may also contribute to the enhanced tumor uptake over the time course. The prolonged *in vivo* half-life of multivalent conjugate is believed to be able to sustain the desired tumor accumulation and retention.[26, 65] However, similar distribution and elimination half-lives were observed for all radiolabeled conjugates. Therefore we think that the observed tumor uptake increase and PET signal amplification was predominately caused by the multivalency of ^{68}Ga-**2** and ^{68}Ga-**3**. It is important to note that the imaging specificity is not compromised because of the added multivalency as it is shown by the complete signal loss in the blockade experiment (Figure 6a and Table S2). The liver signal intensity difference between 2 h and 2 h blockade was likely caused by the diluting effect of the excess cold ligand. However, we acknowledge that the kidney uptake was also increased by the multivalent effect, which might affect how the peptide conjugates are handled in the proximal tubule and their binding to megalin. While the same phenomenon is common in peptide-based radiopharmaceuticals, the exact mechanism for such an increase is unknown. To evaluate the statistic correlation

between the biodistribution and quantitative imaging data, we calculated the Pearson correlation coefficients for all four conjugates. The results (r: ^{68}Ga-**1a** > 0.77; ^{68}Ga-**1** > 0.85; ^{68}Ga-**2** > 0.90; ^{68}Ga-**3** > 0.87) clearly demonstrate a strong correlation.

Conclusions

A series of NOTA-based BFC scaffolds were synthesized to take advantage of multivalent effect for ^{68}Ga PET imaging probe design. Using a well-validated integrin $\alpha_v\beta_3$ ligand, c(RGDyK), peptide conjugates varying multivalency from 1 to 3 were prepared. The *in vitro* and *in vivo* evaluations of the peptide conjugates demonstrated that the preservation of the intact NOTA core in the BFC scaffold design guaranteed rapid and efficient ^{68}Ga incorporation and high *in vivo* stability, while the multivalency rendered by the BFC scaffold design was able to significantly enhance the specific imaging of the targeted $\alpha_v\beta_3$ receptor in a prostate cancer xenograft mouse model. Together with our previously reported BFC scaffold design for ^{64}Cu PET imaging probes, we have validated the design concept that multivalent effect can be realized on a simple BFC scaffold to amplify the desired imaging signal. It is noteworthy that the peptide multimerization method reported by others can be combined with our BFC scaffold design to achieve multi-layered multivalency if necessary. Further, our design allows enhanced specific targeting to heteromeric receptors by incorporating mutually independent targeting molecules on the BFC scaffold.

Supplementary Material

Refer to Web version on PubMed Central for supplementary material.

Acknowledgments

This work was partially supported by a USAMRMC grant (W81XWH-08-1-0305) and two NIH grants (P01 DK058398; U24 CA126608). The authors acknowledge the generous support of a private donor that allowed the purchase of the Inveon PET-CT system.

References

1. Kelloff G, Hoffman JM, Johnson B, Scher HI, Siegel BA, Cheng EY, Cheson BD, O'Shaughnessy J, Guyton KZ, Mankoff DA, Shankar L, Larson SM, Sigman CC, Schilsky RL, Sullivan DC. Progress and promise of FDG-PET imaging for cancer patient management and oncologic drug development. Clin Cancer Res. 2005; 11:2785–2808. [PubMed: 15837727]
2. von Schulthess GK, Steinert HC, Hany TF. Integrated PET/CT-3: Current applications and future directions. Radiology. 2006; 238:405–422. [PubMed: 16436809]
3. Harry VN, Semple SI, Parkin DE, Gilbert FJ. Use of new imaging techniques to predict tumour response to therapy. Lancet Oncol. 2010; 11:92–102. [PubMed: 20129132]
4. de Rosales RTM, Arstad E, Blower PJ. Nuclear imaging of molecular processes in cancer. Target Oncol. 2009; 4:183–197. [PubMed: 19779864]
5. Gambhir SS. Molecular imaging of cancer with positron emission tomography. Nat Rev Cancer. 2002; 2:683–693. [PubMed: 12209157]
6. Phelps ME. Positron emission tomography provides molecular imaging of biological processes. Proceedings of the National Academy of Sciences of the United States of America. 2000; 97:9226–9233. [PubMed: 10922074]
7. Miller PW, Long NJ, Vilar R, Gee AD. Synthesis of ^{11}C, ^{18}F, ^{15}O, and ^{13}N Radiolabels for Positron Emission Tomography. Angew Chem Int Ed. 2008; 47:8998–9033.
8. Pagani M, Stone-Elander S, Larsson SA. Alternative positron emission tomography with non-conventional positron emitters: effects of their physical properties on image quality and potential clinical applications. Eur J Nucl Med Mol Imaging. 1997; 24:1301–1327.

9. Hao G, Singh AN, Liu W, Sun X. PET with Non-Standard Nuclides. Current Topics in Medicinal Chemistry. 2010; 10:1096–1112. [PubMed: 20388114]
10. Al-Nahhas A, Win Z, Szyszko T, Singh A, Khan S, Rubello D. What can gallium-68 PET add to receptor and molecular imaging? Eur J Nucl Med Mol Imaging. 2007; 34:1897–901. [PubMed: 17713764]
11. Al-Nahhas A, Win Z, Szyszko T, Singh A, Nanni C, Fanti S, Rubello D. Gallium-68 PET: a new frontier in receptor cancer imaging. Anticancer Res. 2007; 27:4087–94. [PubMed: 18225576]
12. Khan MU, Khan S, El-Refaie S, Win Z, Rubello D, Al-Nahhas A. Clinical indications for Gallium-68 positron emission tomography imaging. Eur J Surg Oncol. 2009; 35:561–7. [PubMed: 19201567]
13. Schottelius M, Berger S, Poethko T, Schwaiger M, Wester HJ. Development of novel Ga-68- and F-18-labeled GnRH-I analogues with high GnRHR-targeting efficiency. Bioconjugate Chem. 2008; 19:1256–1268.
14. Ehrhardt GJ, Welch MJ. A new germanium-63/gallium-68 generator. J Nucl Med. 1978; 19:925–9. [PubMed: 98618]
15. Jeong JM, Hong MK, Chang YS, Lee Y-S, Kim YJ, Cheon GJ, Lee DS, Chung J-K, Lee MC. Preparation of a promising angiogenesis PET imaging agent: ^{68}Ga-labeled c(RGDyK)-isothiocyanatobenzyl-1,4,7-triazacyclononane-1,4,7-triacetic acid and feasibility studies in mice. J Nucl Med. 2008; 49:830–836. [PubMed: 18413379]
16. Velikyan I, Maecke H, Langstrom B. Convenient Preparation of ^{68}Ga-Based PET-Radiopharmaceuticals at Room Temperature. Bioconjugate Chem. 2008; 19:569–573.
17. Lee J, Garmestani K, Wu C, Brechbiel MW, Chang HK, Choi CW, Gansow OA, Carrasquillo JA, Paik CH. In vitro and in vivo evaluation of structure-stability relationship of ^{111}In- and ^{67}Ga-labeled antibody via 1B4M or C-NOTA chelates. Nucl Med Biol. 1997; 24:225–230. [PubMed: 9228656]
18. Prata MIM, Santos AC, Geraldes CFGC, de Lima JJP. Structural and in vivo studies of metal chelates of Ga(III) relevant to biomedical imaging. J Inorg Biochem. 2000; 79:359–363. [PubMed: 10830889]
19. Prata MI, Santos AC, Geraldes CF, de Lima JJ. Characterisation of $^{67}Ga^{3+}$ complexes of triaza macrocyclic ligands: biodistribution and clearance studies. Nucl Med Biol. 1999; 26:707–10. [PubMed: 10587111]
20. Broan CJ, Cox JPL, Craig AS, Kataky R, Parker D, Harrison A, Randall AM, Ferguson G. Structure and Solution Stability of Indium and Gallium Complexes of 1,4,7-Triazacyclononanetriacetate and of Yttrium Complexes of 1,4,7,10-Tetraazacyclododecanetetraacetate and Related Ligands - Kinetically Stable Complexes for Use in Imaging and Radioimmunotherapy - X-Ray Molecular-Structure of the Indium and Gallium Complexes of 1,4,7-Triazacyclononane-1,4,7-Triacetic Acid. J Chem Soc Perk T. 1991; 2:87–99.
21. Craig AS, Parker D, Adams H, Bailey NA. Stability, Ga-71 Nmr, and Crystal-Structure of a Neutral Gallium(III) Complex of 1,4,7-Triazacyclononanetriacetate - a Potential Radiopharmaceutical. J Chem Soc Chem Comm. 1989:1793–1794.
22. Clarke ET, Martell AE. Stabilities of the Fe(III), Ga(III) and In(III) chelates of N,N′,N″-triazacyclononanetriacetic acid. Inorg Chim Acta. 1991; 181:273–280.
23. Eisenwiener K-P, Prata MIM, Buschmann I, Zhang H-W, Santos AC, Wenger S, Reubi JC, Maecke HR. NODAGATOC, a New Chelator-Coupled Somatostatin Analogue Labeled with [$^{67/68}$Ga] and [^{111}In] for SPECT, PET, and Targeted Therapeutic Applications of Somatostatin Receptor (hsst2) Expressing Tumors. Bioconjugate Chem. 2002; 13:530–541.
24. Andre JP, Maecke HR, Zehnder M, Macko L, Akyel KG. 1,4,7-triazacyclononane-1-succinic acid-4,7-diacetic acid (NODASA): a new bifunctional chelator for radio gallium-labelling of biomolecules. Chem Commun. 1998:1301–1302.
25. Deyev SM, Lebedenko EN. Multivalency: the hallmark of antibodies used for optimization of tumor targeting by design. Bioessays. 2008; 30:904–18. [PubMed: 18693269]
26. Li ZB, Chen K, Chen X. ^{68}Ga-labeled multimeric RGD peptides for microPET imaging of integrin $\alpha_v\beta_3$ expression. Eur J Nucl Med Mol Imaging. 2008; 35:1100–8. [PubMed: 18204838]

27. Liu Z, Niu G, Shi J, Liu S, Wang F, Liu S, Chen X. ^{68}Ga-labeled cyclic RGD dimers with Gly3 and PEG4 linkers: promising agents for tumor integrin $\alpha_v\beta_3$ PET imaging. Eur J Nucl Med Mol Imaging. 2009; 36:947–957. [PubMed: 19159928]
28. Liu W, Hao G, Long Michael A, Anthony T, Hsieh J-T, Sun X. Imparting Multivalency to a Bifunctional Chelator: A Scaffold Design for Targeted PET Imaging Probes. Angew Chem Int Ed. 2009; 48:7346–7349.
29. Eisenwiener KP, Powell P, Macke HR. A convenient synthesis of novel bifunctional prochelators for coupling to bioactive peptides for radiometal labelling. Bioorg Med Chem Lett. 2000; 10:2133–5. [PubMed: 10999487]
30. Welling, PG. Pharmacokinetics: Processes, mathematics, and applications. American Chemical Society; Washington, DC: 1997.
31. Velikyan I, Maecke H, Langstrom B. Convenient preparation of ^{68}Ga-based PET-radiopharmaceuticals at room temperature. Bioconjugate Chem. 2008; 19:569–73.
32. Li ZB, Cai W, Cao Q, Chen K, Wu Z, He L, Chen X. ^{64}Cu-labeled tetrameric and octameric RGD peptides for small-animal PET of tumor $\alpha_v\beta_3$ integrin expression. J Nucl Med. 2007; 48:1162–71. [PubMed: 17574975]
33. Zhang X, Xiong Z, Wu Y, Cai W, Tseng JR, Gambhir SS, Chen X. Quantitative PET Imaging of Tumor Integrin $\alpha_v\beta_3$ Expression with ^{18}F-FRGD2. J Nucl Med. 2006; 47:113–121. [PubMed: 16391195]
34. Montet X, Funovics M, Montet-Abou K, Weissleder R, Josephson L. Multivalent effects of RGD peptides obtained by nanoparticle display. J Med Chem. 2006; 49:6087–93. [PubMed: 17004722]
35. Wadas TJ, Wong EH, Weisman GR, Anderson CJ. Coordinating Radiometals of Copper, Gallium, Indium, Yttrium, and Zirconium for PET and SPECT Imaging of Disease. Chem Rev. 2010; 110:2858–2902. [PubMed: 20415480]
36. Fani M, Andre JP, Maecke HR. ^{68}Ga-PET: a powerful generator-based alternative to cyclotron-based PET radiopharmaceuticals. Contrast Media Mol Imaging. 2008; 3:67–77. [PubMed: 18383558]
37. Maecke HR, Andre JP. ^{68}Ga-PET radiopharmacy: A generator-based alternative to ^{18}F-radiopharmacy. Ernst Schering Res Found Workshop. 2007:215–42. [PubMed: 17172157]
38. Bandoli G, Dolmella A, Tisato F, Porchia M, Refosco F. Mononuclear six-coordinated Ga(III) complexes: A comprehensive survey. Coordin Chem Rev. 2009; 253:56–77.
39. Clarke ET, Martell AE. Stabilities of trivalent metal ion complexes of the tetraacetate derivatives of 12-, 13- and 14-membered tetraazamacrocycles. Inorg Chim Acta. 1991; 190:37–46.
40. Decristoforo C, Hernandez Gonzalez I, Carlsen J, Rupprich M, Huisman M, Virgolini I, Wester HJ, Haubner R. ^{68}Ga- and ^{111}In-labelled DOTA-RGD peptides for imaging of $\alpha_v\beta_3$ integrin expression. Eur J Nucl Med Mol Imaging. 2008; 35:1507–1515. [PubMed: 18369617]
41. Hoigebazar L, Jeong JM, Choi SY, Choi JY, Shetty D, Lee Y-S, Lee DS, Chung J-K, Lee MC, Chung YK. Synthesis and Characterization of Nitroimidazole Derivatives for ^{68}Ga-Labeling and Testing in Tumor Xenografted Mice. J Med Chem. 2010; 53:6378–6385. [PubMed: 20690646]
42. Woods M, Caravan P, Geraldes CF, Greenfield MT, Kiefer GE, Lin M, McMillan K, Prata MI, Santos AC, Sun X, Wang J, Zhang S, Zhao P, Sherry AD. The effect of the amide substituent on the biodistribution and tolerance of lanthanide(III) DOTA-tetraamide derivatives. Invest Radiol. 2008; 43:861–70. [PubMed: 19002058]
43. Brechbiel MW, McMurry TJ, Gansow OA. A direct synthesis of a bifunctional chelating agent for radiolabeling proteins. Tetrahedron Letters. 1993; 34:3691–3694.
44. Cox JPL, Craig AS, Helps IM, Jankowski KJ, Parker D, Eaton MAW, Millican AT, Millar K, Beeley NRA, Boyce BA. Synthesis of C- and N-functionalised derivatives of 1,4,7-triazacyclononane-1,4,7-triyltriacetic acid (NOTA), 1,4,7,10-tetra-azacyclododecane-1,4,7,10-tetrayltetra-acetic acid (DOTA), and diethylenenetriaminepenta-acetic acid (DTPA): bifunctional complexing agents for the derivatisation of antibodies. Journal of the Chemical Society, Perkin Transactions. 1990; 1:2567–2576.
45. McMurry TJ, Brechbiel M, Wu C, Gansow OA. Synthesis of 2-(p-thiocyanatobenzyl)-1,4,7-triazacyclononane-1,4,7-triacetic acid: Application of the 4-methoxy-2,3,6-

trimethylbenzenesulfonamide protecting group in the synthesis of macrocyclic polyamines. Bioconjugate Chem. 1993; 4:236–245.

46. Studer M, Meares CF. Synthesis of novel 1,4,7-triazacyclononane-N,N′,N″-triacetic acid derivatives suitable for protein labeling. Bioconjugate Chem. 1992; 3:337–41.
47. Gestwicki JE, Cairo CW, Strong LE, Oetjen KA, Kiessling LL. Influencing receptor-ligand binding mechanisms with multivalent ligand architecture. J Am Chem Soc. 2002; 124:14922–33. [PubMed: 12475334]
48. Hotez PJ, Bethony JM, Oliveira SC, Brindley PJ, Loukas A. Multivalent anthelminthic vaccine to prevent hookworm and schistosomiasis. Expert Rev Vaccines. 2008; 7:745–52. [PubMed: 18665774]
49. Hudson PJ, Kortt AA. High avidity scFv multimers; diabodies and triabodies. J Immunol Methods. 1999; 231:177–89. [PubMed: 10648937]
50. Reulen SWA, Dankers PYW, Bomans PHH, Meijer EW, Merkx M. Collagen Targeting Using Protein-Functionalized Micelles: The Strength of Multiple Weak Interactions. J Am Chem Soc. 2009; 131:7304–7312. [PubMed: 19469576]
51. Almutairi A, Rossin R, Shokeen M, Hagooly A, Ananth A, Capoccia B, Guillaudeu S, Abendschein D, Anderson CJ, Welch MJ, Fréchet JMJ. Biodegradable dendritic positron-emitting nanoprobes for the noninvasive imaging of angiogenesis. Proc Natl Acad Sci USA. 2009; 106:685–690. [PubMed: 19129498]
52. Hong S, Leroueil PR, Majoros IJ, Orr BG, Baker JR Jr, Banaszak Holl MM. The binding avidity of a nanoparticle-based multivalent targeted drug delivery platform. Chem Biol. 2007; 14:107–15. [PubMed: 17254956]
53. Todorovska A, Roovers RC, Dolezal O, Kortt AA, Hoogenboom HR, Hudson PJ. Design and application of diabodies, triabodies and tetrabodies for cancer targeting. J Immunol Methods. 2001; 248:47–66. [PubMed: 11223068]
54. Ye Y, Bloch S, Xu B, Achilefu S. Design, Synthesis, and Evaluation of Near Infrared Fluorescent Multimeric RGD Peptides for Targeting Tumors. J Med Chem. 2006; 49:2268–2275. [PubMed: 16570923]
55. Chen X, Liu S, Hou Y, Tohme M, Park R, Bading JR, Conti PS. MicroPET imaging of breast cancer α_v-integrin expression with ^{64}Cu-labeled dimeric RGD peptides. Mol Imaging Biol. 2004; 6:350–9. [PubMed: 15380745]
56. Dijkgraaf I, Rijnders AY, Soede A, Dechesne AC, Esse GWv, Brouwer AJ, Corstens FHM, Boerman OC, Rijkers DTS, Liskamp RMJ. Synthesis of DOTA-conjugated multivalent cyclic-RGD peptide dendrimers via 1,3-dipolar cycloaddition and their biological evaluation: implications for tumor targeting and tumor imaging purposes. Organic & Biomolecular Chemistry. 2007; 5:935–944. [PubMed: 17340009]
57. Jia B, Liu Z, Shi J, Yu Z, Yang Z, Zhao H, He Z, Liu S, Wang F. Linker effects on biological properties of ^{111}In-labeled DTPA conjugates of a cyclic RGDfK dimer. Bioconjugate Chem. 2008; 19:201–10.
58. Thumshirn G, Hersel U, Goodman SL, Kessler H. Multimeric cyclic RGD peptides as potential tools for tumor targeting: solid-phase peptide synthesis and chemoselective oxime ligation. Chemistry. 2003; 9:2717–25. [PubMed: 12772286]
59. Liu S. Radiolabeled multimeric cyclic RGD peptides as integrin $\alpha_v\beta_3$ targeted radiotracers for tumor imaging. Mol Pharm. 2006; 3:472–87. [PubMed: 17009846]
60. Liu S. Radiolabeled cyclic RGD peptides as integrin $\alpha_v\beta_3$-targeted radiotracers: maximizing binding affinity *via* bivalency. Bioconjugate Chem. 2009; 20:2199–213.
61. Dijkgraaf I, Kruijtzer JA, Liu S, Soede AC, Oyen WJ, Corstens FH, Liskamp RM, Boerman OC. Improved targeting of the $\alpha_v\beta_3$ integrin by multimerisation of RGD peptides. Eur J Nucl Med Mol Imaging. 2007; 34:267–73. [PubMed: 16909226]
62. Janssen M, Oyen WJ, Massuger LF, Frielink C, Dijkgraaf I, Edwards DS, Radjopadhye M, Corstens FH, Boerman OC. Comparison of a monomeric and dimeric radiolabeled RGD-peptide for tumor targeting. Cancer Biother Radiopharm. 2002; 17:641–6. [PubMed: 12537667]
63. Wang J, Kim YS, Liu S. 99mTc-labeling of HYNIC-conjugated cyclic RGDfK dimer and tetramer using EDDA as coligand. Bioconjugate Chem. 2008; 19:634–42.

64. Zhang X, Liu H, Miao Z, Kimura R, Fan F, Cheng Z. Macrocyclic chelator assembled RGD multimers for tumor targeting. Bioorg Med Chem Lett. 2011; 21:3423–3426. [PubMed: 21524578]

65. Nasongkla N, Chen B, Macaraeg N, Fox ME, Frechet JMJ, Szoka FC. Dependence of Pharmacokinetics and Biodistribution on Polymer Architecture: Effect of Cyclic versus Linear Polymers. J Am Chem Soc. 2009; 131:3842–3843. [PubMed: 19256497]

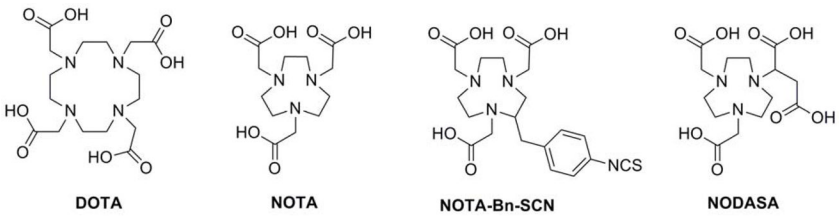

Figure 1.
Structures of commonly used BFCs for gallium radiopharmaceuticals.

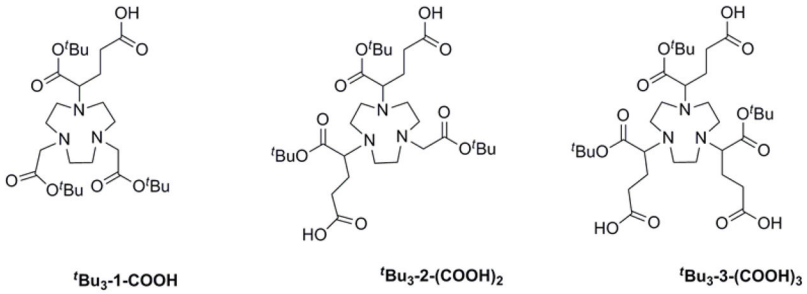

Figure 2.
Structures of ^{t}Bu-protected BFC scaffolds: ^{t}Bu$_3$-**1**-COOH, *t*Bu$_3$-**2**-(COOH)$_2$, and *t*Bu$_3$-**3**-(COOH)$_3$.

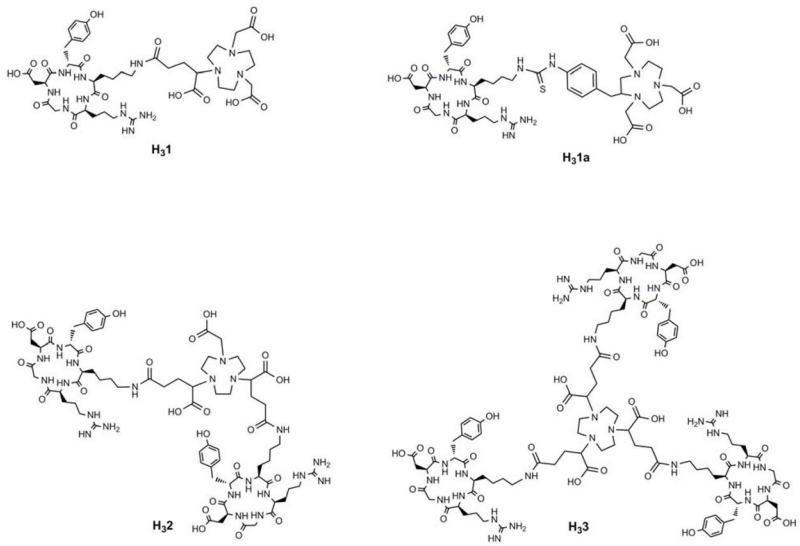

Figure 3.
Structures of peptide conjugates: H_3**1**, H_3**1a**, H_3**2** and H_3**3**.

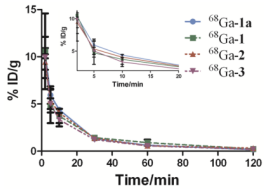

Figure 4.
The time activity curves of ^{68}Ga-**1**, ^{68}Ga-**1a**, ^{68}Ga-**2** and ^{68}Ga-**3**. Data obtained from mouse blood sampling are presented as %ID/g ± s.d. (n = 3).

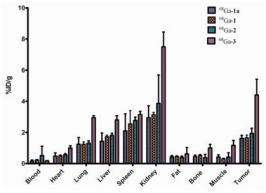

Figure 5.
Tissue distribution of ^{68}Ga-**1**, ^{68}Ga-**1a**, ^{68}Ga-**2** and ^{68}Ga-**3** in PC-3 tumor bearing SCID mice at 2 h p.i. Data are presented as %ID/g ± s.d. (n = 3).

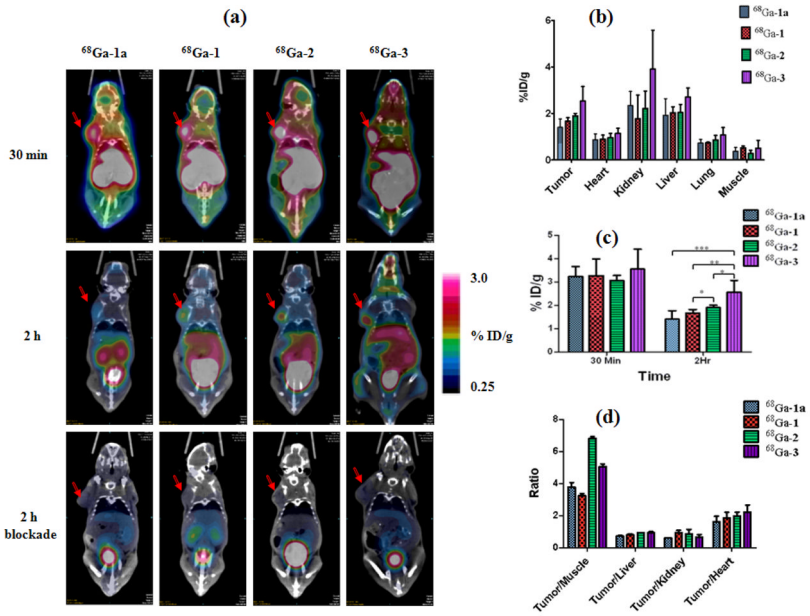

Figure 6.

(a) Decay-corrected whole-body coronal microPET images of SCID mice bearing PC-3 tumor xenograft with ^{68}Ga-**1**, ^{68}Ga-**1a**, ^{68}Ga-**2** and ^{68}Ga-**3**: 30 min (dynamic frame of 25 – 30 min); 2 h (static scan); and 2 h blockade (co-injection with 10-mg/kg of c(RGDyK)). Tumors are indicated by red arrow. For comparison, the images are shown at the same signal intensity scale; (b) Uptake of the ^{68}Ga labeled conjugates at 2 h p.i. in tumor and major organs obtained from quantitative imaging analysis. Data are presented as %ID/g ± s.d. (n = 3); (c) Comparative tumor uptake of the ^{68}Ga labeled conjugates at 30 min and 2 h p.i. Data are presented as %ID/g ± s.d. (n = 3); (d) Ratios of tumor to major organs for the ^{68}Ga labeled conjugates.

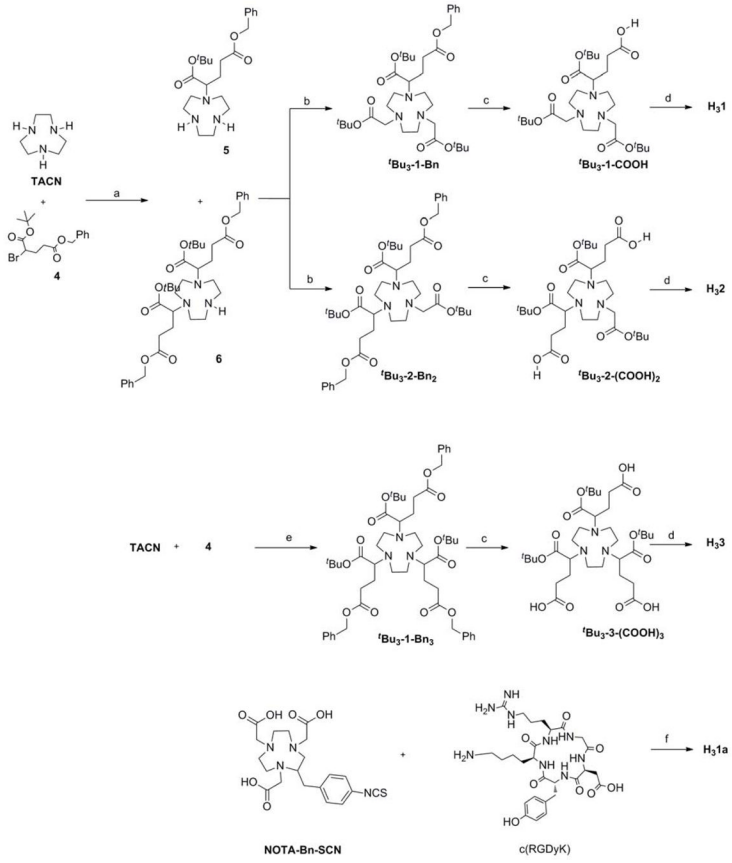

Scheme 1.

Synthetic routes to H_3**1,** H_3**1a,** H_3**2,** and H_3**3**.

(a) $CHCl_3$; (b) MeCN, K_2CO_3, *t*-butyl-2-bromoacetate; (c) 2-propanol, 10% Pd/C, H_2; (d) i- NHS, EDC.HCl, DIPEA; ii- c(RGDyK), DIPEA, DMF; iii- TFA; (e) MeCN, K_2CO_3; (f) DIPEA, DMF.

Table 1

In vivo pharmacokinetic parameters of ^{68}Ga-**1**, ^{68}Ga-**1a**, ^{68}Ga-**2** and ^{68}Ga-**3**.

Conjugates	$t_{1/2(\alpha)}$, min.	$t_{1/2(\beta)}$, min.
^{68}Ga -**1a**	4.0 ± 1.1	29.8 ± 7.1
^{68}Ga -**1**	2.7 ± 0.0	32.9 ± 8.0
^{68}Ga -**2**	3.8 ± 1.4	48.2 ± 9.0
^{68}Ga -**3**	3.4 ± 0.9	36.8 ± 1.1